ARTICLE

doi:10.1038/nature12777

Dedifferentiation of committed epithelial cells into stem cells *in vivo*

Purushothama Rao Tata[1,2,3,4], Hongmei Mou[1,2,3,4], Ana Pardo-Saganta[1,2,3,4], Rui Zhao[1,2,3,4], Mythili Prabhu[1,2,3,4], Brandon M. Law[1,2,3,4], Vladimir Vinarsky[1,2,3,4], Josalyn L. Cho[3,5], Sylvie Breton[6], Amar Sahay[1,4,7], Benjamin D. Medoff[3,5] & Jayaraj Rajagopal[1,2,3,4]

Cellular plasticity contributes to the regenerative capacity of plants, invertebrates, teleost fishes and amphibians. In vertebrates, differentiated cells are known to revert into replicating progenitors, but these cells do not persist as stable stem cells. Here we present evidence that differentiated airway epithelial cells can revert into stable and functional stem cells *in vivo*. After the ablation of airway stem cells, we observed a surprising increase in the proliferation of committed secretory cells. Subsequent lineage tracing demonstrated that the luminal secretory cells had dedifferentiated into basal stem cells. Dedifferentiated cells were morphologically indistinguishable from stem cells and they functioned as well as their endogenous counterparts in repairing epithelial injury. Single secretory cells clonally dedifferentiated into multipotent stem cells when they were cultured *ex vivo* without basal stem cells. By contrast, direct contact with a single basal stem cell was sufficient to prevent secretory cell dedifferentiation. In analogy to classical descriptions of amphibian nuclear reprogramming, the propensity of committed cells to dedifferentiate is inversely correlated to their state of maturity. This capacity of committed cells to dedifferentiate into stem cells may have a more general role in the regeneration of many tissues and in multiple disease states, notably cancer.

The term dedifferentiation was first coined to describe the process in which cells of the urodele retinal pigment epithelium lose their differentiated properties to replace extirpated lens cells[1]. Although not formally demonstrated, the term was used to suggest that differentiated epithelial cells reverted to a previous developmental stage before their subsequent differentiation into an alternative cell fate. Dedifferentiation has since been explored in plants, invertebrates, teleost fishes and amphibians[2–17]. In vertebrates, quiescent differentiated cells can revert into replicating progenitor cells[5–7,11,12,14] to replace lost cells, but these progenitor cells do not persist as stable stem cells[11]. Indeed, in murine hair follicle regeneration, the immediate differentiated progeny of epithelial stem cells are already resistant to dedifferentiation[17]. Conversely, the undifferentiated secretory progenitors of the intestine that are the immediate progeny of intestinal stem cells are able to dedifferentiate into stem cells after injury[13], mimicking the capacity for dedifferentiation of the immediate progeny of *Drosophila* germline stem cells[3,15,16]. Recently, using stringent lineage-tracing strategies[18], airway epithelial cells have been shown to be more plastic than recognized previously. In a separate study, differentiated secretory cells have been shown to give rise to very rare cells ($0.34 \pm 0.09\%$) that express basal cell markers after severe injury, but the properties of these rare basal-like cells were not studied and their functional capacity was not assessed[19]. Here, we specifically sought to determine whether stably committed luminal cells could dedifferentiate into functional stem cells.

Secretory cells replicate after stem cell ablation

Airway basal stem cells have been shown to self-renew and differentiate into multiple airway epithelial cell types using genetic lineage tracing[20,21]. Secretory cells are differentiated luminal cells that have both secretory and detoxifying functions. Secretory cells can also further differentiate into ciliated cells[19]. To test whether secretory cells can dedifferentiate into stem cells, we ablated basal stem cells of the airway epithelium and simultaneously lineage traced the secretory cells of the same mouse (Extended Data Fig. 1). To ablate the airway basal stem cells, we generated a *CK5-rtTA/tet(O)DTA*[22,23] (hereafter referred to as CK5-DTA) mouse, which expresses the active subunit of the diphtheria toxin (DTA) in CK5 (also known as KRT5)$^+$ airway basal stem cells following doxycycline administration. *CK5* expression is, however, not restricted to the basal stem cells of the airway epithelium and is expressed in many other epithelial tissues[20,22]. Therefore, the ablation of *CK5*-expressing cells using systemic doxycycline administration through drinking water or by intraperitoneal injection is lethal in the adult mouse (data not shown). To circumvent this problem, we designed a method for the inhalational delivery of doxycycline[24] as a means of inducing DTA transgene expression exclusively in the airway epithelium. CK5-DTA mice were exposed to either inhaled PBS (i-PBS) or inhaled doxycycline (i-Dox) for two or three consecutive days (Fig. 1a, b). Tracheas were isolated 24 h after the final dose of i-Dox. Immunofluorescence analysis using the basal stem cell markers p63 (also known as TP63), CK5, NGFR and T1α (also known as PDPN) demonstrated a specific dose-dependent ablation of basal cells and a preservation of normal secretory cell numbers (Fig. 1c, d and Extended Data Fig. 2a–c). Approximately 80% ($n = 3$) of the airway basal cells were ablated after three doses of inhaled doxycycline (an $81.0 \pm 3.4\%$ decrease in the number of CK5$^+$ cells and a $78.8 \pm 2.4\%$ decrease in the number of p63$^+$ cells) (Extended Data Fig. 2d). Immunofluorescence staining of the proliferation marker Ki67 in combination with cell-type-specific markers demonstrated that residual CK5$^+$ and p63$^+$ basal cells do proliferate, but there are actually fewer numbers of proliferating basal cells relative

[1]Center for Regenerative Medicine, Massachusetts General Hospital, 185 Cambridge Street, Boston, Massachusetts 02114, USA. [2]Departments of Pediatrics, Massachusetts General Hospital, Boston, Massachusetts 02114, USA. [3]Department of Internal Medicine, Pulmonary and Critical Care Unit, Massachusetts General Hospital, Boston, Massachusetts 02114, USA. [4]Harvard Stem Cell Institute, Cambridge, Massachusetts 02138, USA. [5]Center for Immunology and Inflammatory Diseases, Massachusetts General Hospital, Charlestown, Massachusetts 02129, USA. [6]Center for Systems Biology, Program in Membrane Biology and Nephrology Division, Massachusetts General Hospital and Harvard Medical School, Boston, Massachusetts 02214, USA. [7]Department of Psychiatry, Harvard Medical School, Boston, Massachusetts 02215, USA.

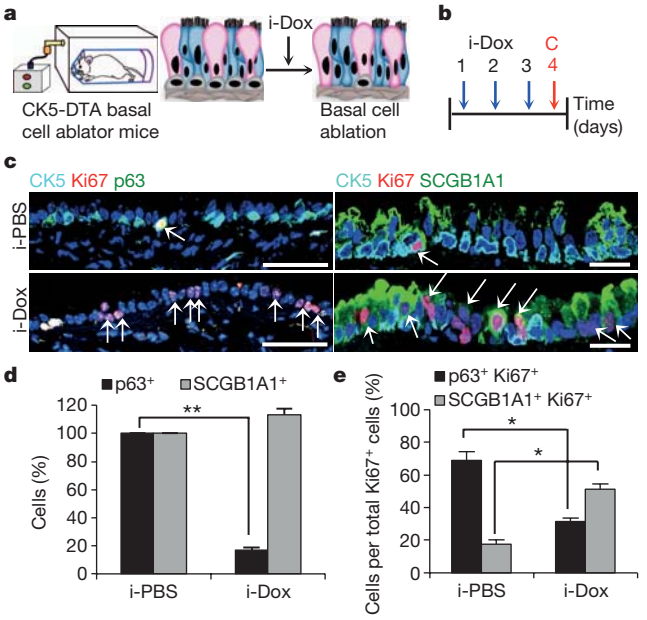

Figure 1 | Secretory cells proliferate after basal cell ablation. **a**, Schematic representation of the ablation of *CK5*-expressing basal cells of the trachea. Secretory, ciliated and basal stem cells are shown in pink, blue and grey, respectively. **b**, Schematic of the timeline of i-Dox or i-PBS administration and tissue collection (C). **c**, Immunostaining for basal (p63 (green) and CK5 (cyan)) and secretory cells (SCGB1A1 (green)) in combination with Ki67 (red) on either i-PBS (top)- or i-Dox (bottom)-treated mice ($n = 6$). White arrows, Ki67$^+$ cells. **d**, Quantification of the percentage of p63$^+$ and SCGB1A1$^+$ cells per total number of DAPI (4′,6-diamidino-2-phenylindole)-stained epithelial cells in i-PBS or i-Dox groups. $n = 3$. **e**, Percentage of p63$^+$ Ki67$^+$ and SCGB1A1$^+$ Ki67$^+$ cells relative to total Ki67$^+$ cells in i-PBS- and i-Dox ($n = 3$)-treated CK5-DTA mice. Nuclei, DAPI (blue). $^*P < 0.05$, $^{**}P < 0.01$ (two tailed and paired *t*-test). $n = 3$ (three mice per condition). Error bars, average ± s.e.m. Scale bars, 20 µm.

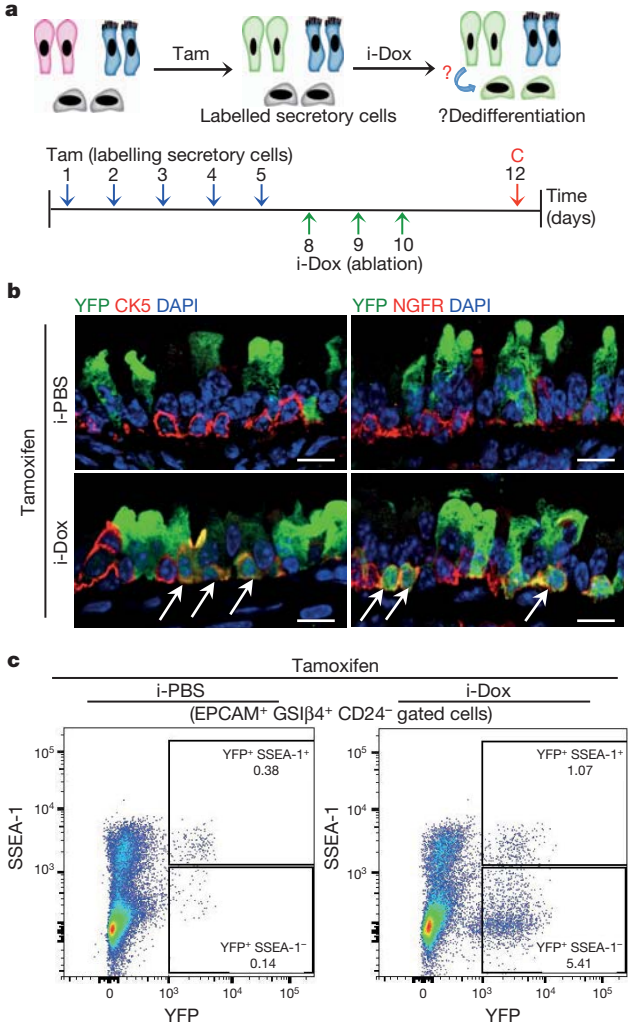

Figure 2 | Luminal secretory cells dedifferentiate into basal stem cells after stem-cell ablation. **a**, Schematic representation of tamoxifen (Tam) and i-Dox administration to SCGB1A1–YFP/CK5-DTA mice followed by tissue collection (C). **b**, Immunostaining for CK5 (red; left) and NGFR (red; right) in combination with YFP (green) in i-PBS (top)- or i-Dox (bottom)-treated mice ($n = 3$). White arrows indicate double-positive cells. **c**, Flow-cytometric analysis of dedifferentiated cells. EPCAM$^+$ GSIβ4$^+$ CD24$^-$ cells were analysed for expression of SSEA-1 and YFP in either i-Dox- or i-PBS-treated mice. $n = 3$ (at least two mice each per condition). Scale bars, 20 µm.

to the total population of replicating cells after ablation (Fig. 1c, e). Notably, there was a twofold increase in the numbers of replicating secretory cells (SCGB1A1$^+$ Ki67$^+$) in i-Dox-treated animals (51.29 ± 3.02%) as compared to i-PBS-treated animals (17.7 ± 2.68%) (Fig. 1c, e and Extended Data Fig. 3a). Consistent with the increased proliferation of differentiated secretory cells, Ki67 staining was specifically increased in the CK8 (also known as KRT8)$^+$ suprabasal layer of the airway epithelium (Extended Data Fig. 3b). Thus, secretory cells are the predominant cells that replicate after stem cell ablation. Interestingly, occasional cells expressed both the basal cell marker CK5 and the secretory cell marker SCGB1A1 in i-Dox-treated mice (Extended Data Fig. 3c).

Secretory cells dedifferentiate *in vivo*

To lineage-label secretory cells before stem cell ablation, we generated quadruple transgenic mice: *Scgb1a1-creER/LSL-YFP::CK5-rtTA-tet(O)DTA* (hereafter referred to as SCGB1A1–YFP/CK5-DTA mice). Administration of tamoxifen to induce the CreER-mediated expression of the yellow fluorescent protein (YFP) label in secretory cells was followed by three doses of i-Dox to induce basal cell ablation (Fig. 2a). Lineage-labelled YFP$^+$ secretory cells demonstrated increased rates of proliferation in i-Dox-treated animals as compared to i-PBS treated controls (Extended Data Fig. 3d, e). We identified YFP$^+$ secretory-cell-derived cells that were morphologically indistinguishable from basal stem cells (Fig. 2b). In addition, we found that a subset of lineage-labelled cells expressed a suite of basal cell markers including CK5, NGFR, p63 and T1α (Fig. 2b and Extended Data Fig. 3f). Quantification revealed that 7.9 ± 2.08% of basal cells (585 CK5$^+$ YFP$^+$ cells out of 7,320 total CK5$^+$ cells in i-Dox-treated animals, $n = 6$ mice) expressed a YFP lineage label, demonstrating that dedifferentiated basal-like cells comprised a substantial fraction of the total stem cell pool. Dedifferentiated cells did not appear in PBS-treated controls (3 CK5$^+$ YFP$^+$ cells out of 7,558 total CK5$^+$ cells counted (0.041 ± 0.028%; $n = 6$ mice)). Consistently, when the entire basal cell population is purified by flow cytometry, the YFP-lineage-labelled basal-like cells have lost the secretory cell surface marker SSEA-1 (Fig. 2c). Thus, dedifferentiating cells lose markers of secretory cell differentiation as they acquire markers of basal stem cells.

Secretory cells dedifferentiate *ex vivo*

Because our *in vivo* experiments demonstrated that secretory cells are stimulated to dedifferentiate by the ablation of basal stem cells, we wondered whether secretory cell dedifferentiation could be induced *ex vivo* when secretory cells were cultured in the absence of basal stem cells. We reasoned that such an assay would provide a platform for further determining whether the dedifferentiation process is actively suppressed by the presence of co-cultured basal stem cells. To assess this possibility, we isolated and sorted unlabelled basal stem cells and YFP$^+$ secretory cells from SCGB1A1–YFP mice after tamoxifen

injection (Extended Data Fig. 4). We then performed sphere-forming assays with these pure YFP-labelled secretory cells alone or in combination with pure sorted GSIβ4$^+$ unlabelled basal cells in varying proportions. The formation of three possible types of spheres is predicted to occur, including spheres that are comprised of (1) exclusively YFP$^+$ secretory-cell-derived cells; (2) exclusively unlabelled basal-cell-derived cells; or (3) chimaeric spheres containing YFP$^+$ secretory-cell-derived and unlabelled basal-cell-derived cells in the same sphere (Fig. 3a). Using our mixed cell populations, we identified a seeding density at which 99.14% ± 0.18 ($n = 3$) of spheres were either entirely YFP$^+$ or entirely unlabelled, thus establishing a clonal origin of the spheres. Regardless of the relative ratio of input secretory and basal stem cells cultured together in a well, the aggregate clonal sphere-forming efficiency of each cell type remained constant (Fig. 3b). Immunofluorescence analysis demonstrated that in many spheres originating from a single YFP$^+$ secretory cell, some YFP$^+$ cells expressed the basal stem cell markers CK5 and p63, indicating that secretory cell dedifferentiation occurs *ex vivo* (even in the presence of nearby purely stem-cell-derived spheres; Fig. 3c). Thus, we established an *ex vivo* clonal dedifferentiation assay. Of the total spheres derived clonally from YFP$^+$ secretory cells, 88% showed evidence of dedifferentiation, and in 70.58% of these spheres, more than 10% of cells expressed the stem cell marker CK5. Even when the input proportion of basal cells to secretory cells plated in Matrigel was 100:1, no inhibition of dedifferentiation was observed in the spheres that were clonally derived from secretory cells (data not shown). This suggested the possibility that basal cells in one sphere do not provide a secreted factor to suppress the dedifferentiation of secretory cells in another sphere and that direct contact is required to suppress secretory cell dedifferentiation. Indeed, we observed that in the small fraction (0.86% ± 0.09; $n = 3$) of chimaerically derived spheres, not a single YFP$^+$-labelled secretory cell dedifferentiated and went on to express basal cell markers (Fig. 3c). Therefore a single basal stem cell in direct contact with a secretory cell prevents dedifferentiation. Of note, these findings cannot entirely exclude the possibility that a secreted stem-cell-derived growth factor can locally suppress secretory cell dedifferentiation. However, they do suggest that an intimate association of basal cells and secretory cells would be required to generate sufficient concentrations of a putative secreted dedifferentiation-suppressing activity.

To provide further confirmation that secretory cells can dedifferentiate into basal cells *ex vivo*, we used mice carrying a doxycycline-inducible basal-cell-specific reporter allele (*CK5-rtTA/tet(O)H2BGFP*) and sorted SSEA-1$^+$/H2B–GFP (in which the human histone H2B coding sequence is fused to the GFP coding sequence)$^-$ secretory cells from their tracheas (Extended Data Fig. 5a, b) and performed a sphere-forming assay. We verified that no GFP$^+$ cells were present before induction by doxycycline. When doxycycline was administered during the course of sphere formation, the first appearance of H2B–GFP occurred at day 3 of culture, indicating that the secretory cells had been converted into basal-like cells. Immunofluorescence analysis revealed that the resulting H2B–GFP$^+$ cells also expressed p63 and CK5 (Extended Data Fig. 5c, left panels). The same results were obtained when the sorted SSEA-1$^+$/H2B–GFP$^-$ cells were grown on transwells (Extended Data Fig. 5c, right panels). In addition, secretory cells also dedifferentiated into basal-like cells when we cultured lineage-labelled YFP$^+$ cells of SCGB1A1–YFP mice on transwell membranes or as spheres (Extended Data Fig. 6a–d). These *ex vivo*-dedifferentiated cells could be serially passaged five times in transwell culture or as spheres and retain their expression of basal stem cell markers and their ability to self-renew (Extended Data Fig. 6d, e). Similarly, cells that had undergone dedifferentiation *in vivo* could also be passaged as stable stem cells (Extended Data Fig. 6f, g). Thus, dedifferentiated secretory cells can stably self-renew.

Mature secretory cells resist dedifferentiation

To determine whether all secretory cells have the potential to dedifferentiate or whether only a subset of secretory cells is endowed with this capacity, we attempted to subset this class of epithelial cells. To do so, we made use of a transgenic mouse strain that expresses enhanced green fluorescent protein (eGFP) specifically in secretory cells of the

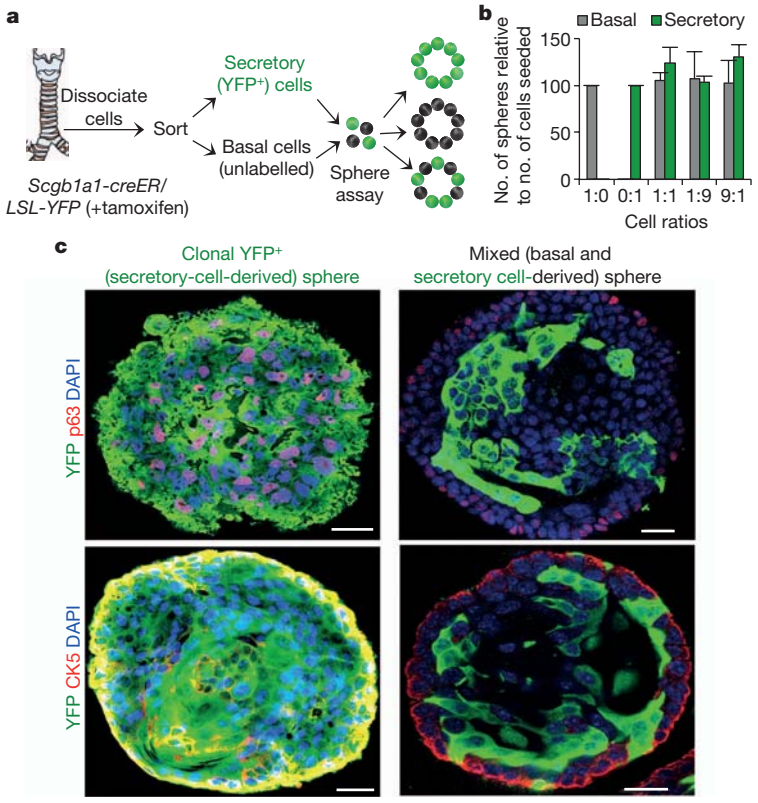

Figure 3 | Secretory cells dedifferentiate in the absence of basal cells in an *ex vivo* sphere-forming assay. **a**, Schematic representation of lineage labelling, sorting and *ex vivo* sphere-forming assay. Schematic representation of different types of spheres anticipated from the basal and secretory cell-mixing assay. **b**, Quantification of the number of spheres that are either basal-cell-derived (grey bars) and secretory-cell-derived (green bars). *x* axis, the ratios of basal to secretory cells seeded. *y* axis, number of spheres formed relative to the number of cells seeded. **c**, Immunostaining for p63 (red; top) or CK5 (red; bottom) in combination with YFP (green). $n = 3$ (two replicates per condition). Error bars, average ± s.e.m. Scale bars, 20 μm.

airway epithelium driven by the promoter of the B1 subunit of the vacuolar H(+)-ATPase gene (*Atp6v1b1*; which we reasoned would be associated with mature secretory cells and hereafter refer to as B1–eGFP)[25,26]. Co-immunostaining for SSEA-1 and GFP demonstrated the existence of three subpopulations of secretory cells: SSEA-1$^+$/GFP$^-$, SSEA-1$^+$/GFP$^+$ and SSEA-1$^-$/GFP$^+$ (Extended Data Fig. 7a). Of note, all GFP$^+$ cells are SCGB1A1$^+$ secretory cells and none are CK5$^+$ basal cells (Extended Data Fig. 7a). To define the cellular hierarchy of these three subsets of cells, we exposed the airway epithelium of B1–eGFP mice to sulphur dioxide (SO_2) injury. In this injury model, SO_2 causes the complete sloughing of only the suprabasal differentiated cells. The remaining basal stem cells are left intact and start replicating within 24 h to give rise to a mature epithelium within 14 days. We found that single-positive SSEA-1$^+$ cells appeared first on day 4 and then matured into double-positive SSEA-1$^+$/GFP$^+$ cells on day 6 (Extended Data Fig. 7b) before the formation of any fully mature single-positive B1–eGFP$^+$ cells evident in the fully mature homeostatic epithelium (Extended Data Fig. 7a, bottom panel, arrowheads). Using B1–eGFP mice, we performed sphere-forming assays with each of the three subsets of secretory cells (Fig. 4a). Intriguingly, all three subsets of cells formed similar large spheres and all these spheres contained basal-like cells (Fig. 4b–d). Interestingly, the sphere-forming ability of the three populations was inversely proportional to the relative maturity of the secretory cell subsets (Fig. 4d). Of note, most of the cell aggregates produced from the most mature SSEA-1$^-$/GFP$^+$ secretory cell subset occurred as small cell clusters instead of spheres (Fig. 4c, e). Furthermore, these cell clusters did not contain CK5- or p63-expressing basal stem cells (Fig. 4c).

Dedifferentiated cells stably persist

To assess whether dedifferentiated stem-cell-like cells have the ability to self-renew and persist *in vivo*, we generated SCGB1A1–YFP/CK5-DTA mice that possessed lineage-labelled dedifferentiated basal-like cells as above and these mice were then maintained for 2 months before euthanization (Extended Data Fig. 8a). Dedifferentiated YFP$^+$ CK5$^+$ cells persisted and continued to represent a sizeable fraction of the stem cell pool (9.15% ± 0.41; $n = 3$). The relative pool size of dedifferentiated basal-like cells remained stable over the course of 2 months (dedifferentiated basal cells represented 8% of the stem cell pool immediately after dedifferentiation). In addition, triple immunostaining for CK5, YFP and Ki67 revealed that YFP$^+$ CK5$^+$ dedifferentiated basal-like cells have the same self-renewal rates as do their normal YFP$^-$ CK5$^+$ basal stem cell counterparts (Extended Data Fig. 8b, c).

Dedifferentiated cells are functional stem cells

To assess the functional stem cell capacity of dedifferentiated basal-like cells, we generated SCGB1A1–YFP/CK5-DTA mice that possessed lineage-labelled dedifferentiated basal-like cells and then exposed these animals to two forms of physiologic airway injury (Fig. 5a, b). First, a toxin-induced airway injury with inhaled SO_2 was used to efficiently denude suprabasal cells from the airway epithelium, leaving behind a single layer of basal cells, some of which were derived from labelled secretory cells that had dedifferentiated (marked by YFP) (Extended Data Fig. 9a). The epithelium fully regenerated in 14 days as expected and immunofluorescence analysis for YFP in combination with CK5 (basal cell), SCGB1A1 (secretory cell) and FOXJ1 (ciliated cell) revealed that YFP$^+$ cells contributed to all three epithelial cell lineages in the form of scattered YFP$^+$ patches (Fig. 5c, top panels). To further scrutinize the functional potential of our dedifferentiated basal-like cells, we used influenza viral infection as a second physiologic injury model (Extended Data Fig. 9b)[27]. We again observed that dedifferentiated basal-like cells participate in regeneration by giving rise to all three epithelial cell types of the airway (Fig. 5c, bottom panels). Similarly, sorted dedifferentiated cells that were produced either *in vivo* or *ex vivo* could be serially passaged in culture and differentiated into mature airway epithelium (Fig. 5d–f and Extended Data Fig. 10a–c).

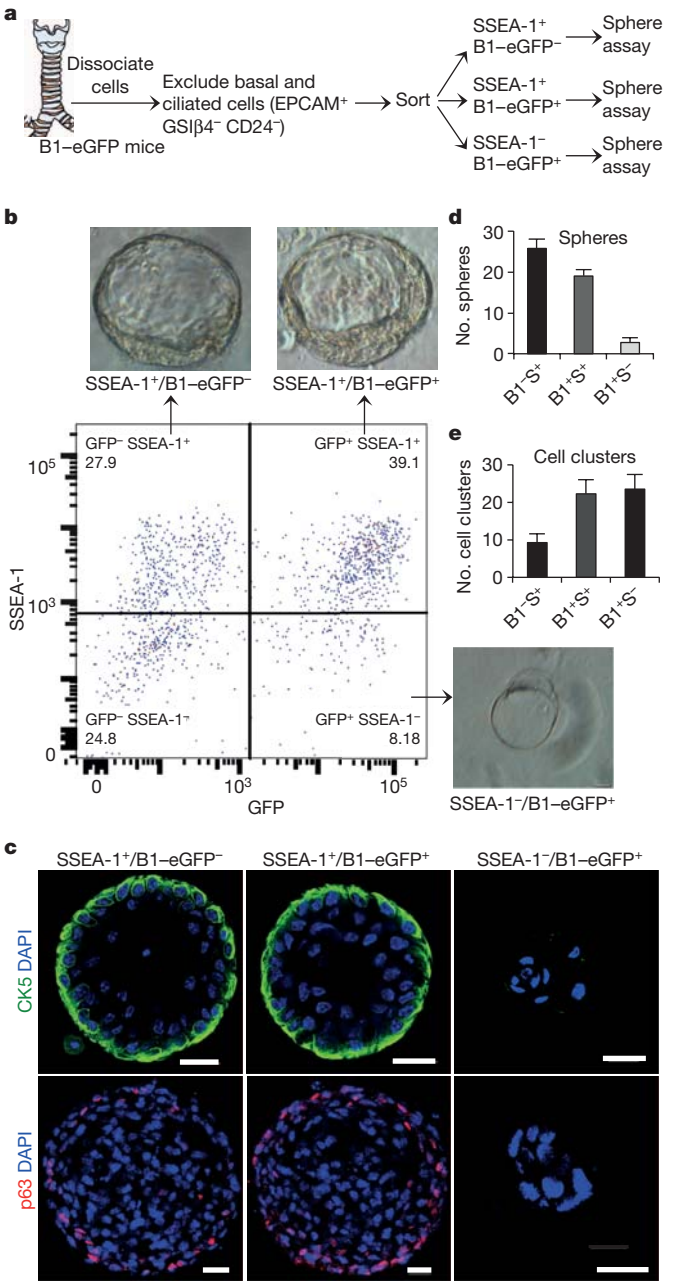

Figure 4 | Dedifferentiation potential of secretory cells is inversely proportional to their maturity. **a**, Schematic representation of dissociation and sorting of three subsets of secretory cells on the basis of SSEA-1 and GFP expression. **b**, Sorting of secretory cell subsets followed by sphere-forming assay. Representative images of the predominant type of cell aggregates (spheres or cell clusters) from secretory cell subsets. **c**, Immunostaining for CK5 (green) and p63 (red) on cell aggregates. **d**, **e**, Quantification of the number of spheres (**d**) or cell clusters (**e**) from secretory cell subsets. $n = 3$ (two replicates per condition). B1, B1–eGFP; S, SSEA-1. Error bars, average ± s.e.m. Scale bars, 20 μm.

Furthermore, we asked whether individual dedifferentiated basal-like cells are multipotent (that is, able to give rise to ciliated, secretory and basal cells) or unipotent (that is, able to give rise to only one of the cell types). To address this issue, we cultured individual dedifferentiated cells and then performed an air–liquid interface culture using these clonally derived stem cells. Immunofluorescence analyses for basal, secretory and ciliated cell markers revealed that most of the clonally derived basal-like cells (11 out of 13 clones) are multipotent (Extended Data Fig. 10d). Intriguingly, rare clones give rise to only

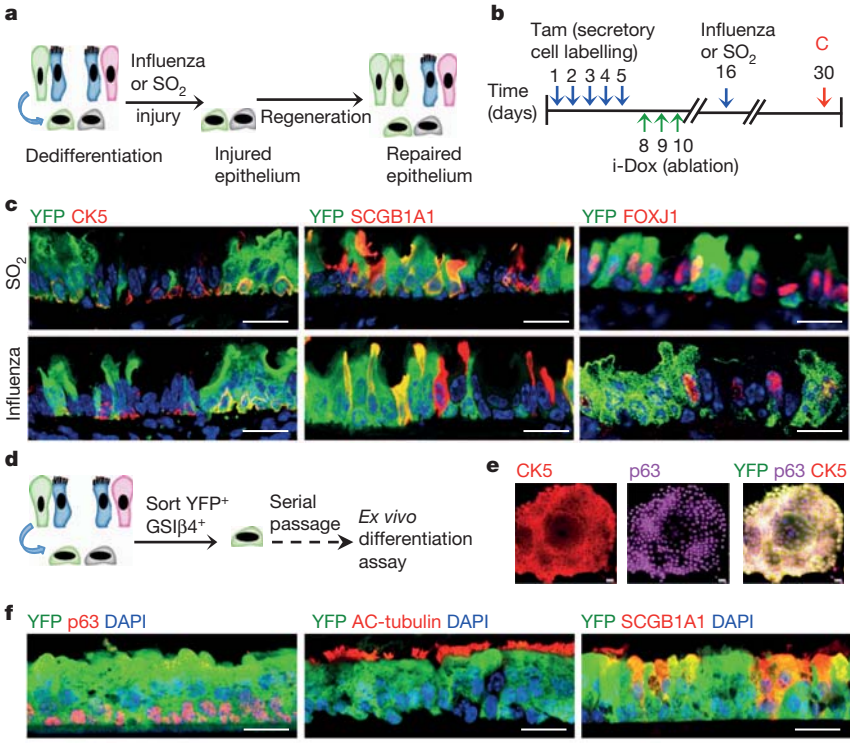

Figure 5 | Dedifferentiated cells are functional stem cells both *in vivo* and *ex vivo*. **a**, Schematic representation of the regeneration of epithelium from dedifferentiated cells after SO_2- or influenza-induced injury. **b**, Timeline for the induction of dedifferentiation before infectious or toxic injury followed by tissue collection (C). **c**, Co-labelling of YFP (green) with CK5 (red; left), SCGB1A1 (red; middle) and FOXJ1 (red; right) after SO_2 (top)- or influenza (bottom)-induced injury. **d**. *Ex vivo* expansion, and differentiation of sorted dedifferentiated cells. **e**, Immunostaining for CK5(red), p63 (magenta) and YFP (green) on colonies from sorted dedifferentiated cells. **f**, Co-labelling of YFP (green) with p63 or acetylated (AC)-tubulin or SCGB1A1 (red). $n = 3$ (two replicates per mouse per condition). Scale bars, 20 μm.

ciliated (1 out of 13 clones) or secretory cells (1 out of 13 clones). The potential of single dedifferentiated cells to act as multipotent stem cells suggests that some or most basal stem cells *in vivo* may analogously serve as multipotent stem cells. However, the rare lineage restricted clones we observe may reflect a heterogeneity in the basal cell population *in vivo* that warrants future scrutiny.

Discussion

Here, using lineage tracing, we have presented evidence that fully differentiated cells can revert into stable and functional basal stem cells. By contrast, in the hair follicle, the committed progeny of skin stem cells do not revert into stem cells when the skin stem cells are ablated[17]. However, in the murine intestinal epithelium, undifferentiated secretory progenitors that are the immediate villin-negative progeny of stem cells can revert back to a stem cell state after injury[13]. Notably, the capacity of fully differentiated villin-positive intestinal secretory cells to revert into stem cells was not assessed. Here we show that fully committed secretory cells respond to stem cell ablation by proliferating and converting into functional epithelial stem cells. Our study points to an alternative cellular mechanism through which tissues can regenerate after stem cell loss. The existence of multiple cellular reservoirs of regenerative capacity may allow a more effective reparative response when one or the other cell type is damaged by a toxic or infectious insult.

The ability of basal stem cells to prevent the dedifferentiation of secretory cells has many implications for tissue biology in general, as stem cells and their progeny can now be seen to reciprocally modulate one another to regulate their relative ratios and thereby overall tissue architecture. In our example, the prevention of secretory cell dedifferentiation occurs through direct contact, even with a single stem cell. This mechanism ensures a precise and local control of epithelial architecture. More generally, it suggests that the reciprocal interactions of stem and committed cells may have been 'designed' to ensure a robust self-organizing property in diverse tissue types.

Furthermore, the ability of differentiated cells to acquire stem cell properties seems to be inversely proportional to the degree of the maturity of the differentiated cells. This is analogous to the results seen in amphibian nuclear reprogramming in which nuclei from more mature cells were less easily reprogrammed than those of their immature counterparts[28,29]. The capacity to segregate secretory cells according to their maturity and associated ability to resist dedifferentiation provides an ideal *in vivo* experimental model for dissecting the molecular mechanisms through which cells might lock their identity as they mature. Finally, our findings have broad implications for cancer biology, as our results point to an underlying physiologic form of cell plasticity that could be co-opted in the process of tumorigenesis[30–34]. Indeed, some lung cancers seem to be able to resist chemotherapy by using a lineage conversion into a different tumour subtype[35].

METHODS SUMMARY

CK5-rtTA[22], *Scgb1a1-creER*[19], *tet(O)DTA*[23] and *B1-eGFP*[25,26] mice were described previously. Corn oil or tamoxifen (2 mg per 20 g body weight) were intraperitoneally injected for five consecutive days. Aerosolized PBS or doxycycline was administered by inhalation[24]. SO_2 injury models have been reported previously[19]. Mice were anesthetized and infected with a sublethal dose of influenza by intranasal inhalation as described previously[27]. Sphere culture and staining was performed as described previously[20]. Immunofluorescence and cell sorting were performed using standard protocols.

Online Content Any additional Methods, Extended Data display items and Source Data are available in the online version of the paper; references unique to these sections appear only in the online paper.

Received 4 April; accepted 17 October 2013.
Published online 6 November 2013.

1. Wolff, G. EntwicklungsphysiologischeStudien. I. Die Regeneration der Urodelenlinse. *Arch. Entwickl. Mech. Org.* **1,** 380–390 (1895).
2. Brockes, J. P. & Kumar, A. Plasticity and reprogramming of differentiated cells in amphibian regeneration. *Nature Rev. Mol. Cell Biol.* **3,** 566–574 (2002).
3. Kai, T. & Spradling, A. Differentiating germ cells can revert into functional stem cells in *Drosophila melanogaster* ovaries. *Nature* **428,** 564–569 (2004).
4. Slack, J. M. W. Metaplasia and transdifferentiation: from pure biology to the clinic. *Nature Rev. Mol. Cell Biol.* **8,** 369–378 (2007).
5. Kragl, M. *et al.* Cells keep a memory of their tissue origin during axolotl limb regeneration. *Nature* **460,** 60–65 (2009).
6. Lehoczky, J. A., Robert, B. & Tabin, C. J. Mouse digit tip regeneration is mediated by fate-restricted progenitor cells. *Proc. Natl Acad. Sci. USA* **108,** 20609–20614 (2011).

7. Rinkevich, Y., Lindau, P., Ueno, H., Longaker, M. T. & Weissman, I. L. Germ-layer and lineage-restricted stem/progenitors regenerate the mouse digit tip. *Nature* **476,** 409–413 (2011).
8. Sugimoto, K., Gordon, S. P. & Meyerowitz, E. M. Regeneration in plants and animals: dedifferentiation, transdifferentiation, or just differentiation? *Trends Cell Biol.* **21,** 212–218 (2011).
9. Wang, X. *et al.* A luminal epithelial stem cell that is a cell of origin for prostate cancer. *Nature* **461,** 495–500 (2009).
10. Van Keymeulen, A. *et al.* Distinct stem cells contribute to mammary gland development and maintenance. *Nature* **479,** 189–193 (2011).
11. Jopling, C. *et al.* Zebrafish heart regeneration occurs by cardiomyocyte dedifferentiation and proliferation. *Nature* **464,** 606–609 (2010).
12. Jopling, C., Boue, S. & Izpisua Belmonte, J. C. Dedifferentiation, transdifferentiation and reprogramming: three routes to regeneration. *Nature Rev. Mol. Cell Biol.* **12,** 79–89 (2011).
13. vanEs, J. H. *et al.* Dll1^{+} secretory progenitor cells revert to stem cells upon crypt damage. *Nature Cell Biol.* **14,** 1099–1104 (2012).
14. Dabeva, M. D. *et al.* Liver regeneration and α-fetoprotein messenger RNA expression in the retrorsine model for hepatocyte transplantation. *Cancer Res.* **58,** 5825–5834 (1998).
15. Brawley, C. & Matunis, E. Regeneration of male germline stem cells by spermatogonial dedifferentiation *in vivo*. *Science* **304,** 1331–1334 (2004).
16. Cheng, J. *et al.* Centrosome misorientation reduces stem cell division during ageing. *Nature* **456,** 599–604 (2008).
17. Hsu, Y., -C., Pasolli, H. A. & Fuchs, E. Dynamics between stem cells, niche, and progeny in the hair follicle. *Cell* **144,** 92–105 (2011).
18. Song, H. *et al.* Functional characterization of pulmonary neuroendocrine cells in lung development, injury, and tumorigenesis. *Proc. Natl Acad. Sci. USA* **109,** 17531–17536 (2012).
19. Rawlins, E. L. *et al.* The role of Scgb1a1^{+} Clara cells in the long-term maintenance and repair of lung airway, but not alveolar, epithelium. *Cell Stem Cell* **4,** 525–534 (2009).
20. Rock, J. R. *et al.* Basal cells as stem cells of the mouse trachea and human airway epithelium. *Proc. Natl Acad. Sci. USA* **106,** 12771–12775 (2009).
21. Rock, J. R. & Hogan, B. L. M. Epithelial progenitor cells in lung development, maintenance, repair, and disease. *Annu. Rev. Cell Dev. Biol.* **27,** 493–512 (2011).
22. Diamond, I., Owolabi, T., Marco, M., Lam, C. & Glick, A. Conditional gene expression in the epidermis of transgenic mice using the tetracycline-regulated transactivatorstTA and rTA linked to the keratin 5 promoter. *J. Invest. Dermatol.* **115,** 788–794 (2000).
23. Weber, T. *et al.* Inducible gene expression in GFAP^{+} progenitor cells of the SGZ and the dorsal wall of the SVZ—a novel tool to manipulate and trace adult neurogenesis. *Glia* **59,** 615–626 (2011).
24. Tata, P. R. *et al.* Airway specific inducible transgene expression using aerosolized doxycycline. *Am. J. Respir. Cell Mol. Biol.* http://dx.doi.org/10.1165/rcmb.2012-0412OC (12 July, 2013).
25. Miller, R. L. *et al.* V-ATPase B1-subunit promoter drives expression of EGFP in intercalated cells of kidney, clear cells of epididymis and airway cells of lung in transgenic mice. *Am. J. Physiol. Cell Physiol.* **288,** C1134–C1144 (2005).
26. Kim, J. K. *et al. In vivo* imaging of tracheal epithelial cells in mice during airway regeneration. *Am. J. Respir. Cell Mol. Biol.* **47,** 864–868 (2012).
27. Cho, J. L. *et al.* Enhanced Tim3 activity improves survival after influenza infection. *J. Immunol.* **189,** 2879–2889 (2012).
28. Briggs, R. & King, T. J. Transplantation of living nuclei from blastula cells into enucleated frogs' eggs. *Proc. Natl Acad. Sci. USA* **38,** 455–463 (1952).
29. Gurdon, J. B., Elsdale, T. R. & Fischberg, M. Sexually mature individuals of *Xenopus laevis* from the transplantation of single somatic nuclei. *Nature* **182,** 64–65 (1958).
30. Blanpain, C. Tracing the cellular origin of cancer. *Nature Cell Biol.* **15,** 126–134 (2012).
31. Schwitalla, S. *et al.* Intestinal tumorigenesis initiated by dedifferentiation and acquisition of stem-cell-like properties. *Cell* **152,** 25–38 (2013).
32. Friedmann-Morvinski, D. *et al.* Dedifferentiation of neurons and astrocytes by oncogenes can induce gliomas in mice. *Science* **338,** 1080–1084 (2012).
33. Visvader, J. E. Cells of origin in cancer. *Nature* **469,** 314–322 (2011).
34. Goldstein, A. S., Huang, J., Guo, C., Garraway, I. P. & Witte, O. N. Identification of a cell of origin for human prostate cancer. *Science* **329,** 568–571 (2010).
35. Sequist, L. V. *et al.* Genotypic and histological evolution of lung cancers acquiring resistance to EGFR inhibitors. *Sci. Transl. Med.* **3,** 75ra26 (2011).

Acknowledgements The work in this manuscript was supported by a Harvard Stem Cell Institute Seed Grant and a National Institutes of Health-National Heart, Lung, and Blood Institute Early Career Research New Faculty (P30) award (5P30HL101287-02) and a Harvard Stem Cell Institute (HSCI) Junior Investigator Grant to J.R. J.R. is a New York Stem Cell Foundation-Robertson Investigator. We wish to extend our thanks to W. Anderson, Y. Dor, Q. Zhou, A. Brack, J. Galloway and all members of the Rajagopal laboratory for their constructive criticism. We thank the members of the HSCI flow cytometry core facility for help with cell sorting.

Author Contributions P.R.T. designed and performed experiments and wrote the manuscript; H.M., A.P.-S., R.Z., M.P., B.M.L. and V.V. performed *ex vivo* experiments; J.L.C. performed influenza infection experiments; A.S. provided *tet(O)DTA* mice and edited the manuscript; S.B. provided *B1-eGFP* mice; B.D.M. reviewed the manuscript; J.R. suggested and co-designed the study and co-wrote the manuscript with P.R.T.

Author Information Reprints and permissions information is available at www.nature.com/reprints. The authors declare no competing financial interests. Readers are welcome to comment on the online version of the paper. Correspondence and requests for materials should be addressed to J.R. (jrajagopal@partners.org).

METHODS

Mouse models. *CK5-rtTA*[22], *Scgb1a1-creER*[19], *tet(O)DTA*[23] and *B1-eGFP*[25,26] mice were described previously. *Rosa26R-eYFP (Gt(Rosa)26Sor$^{tm1(eYFP)Cos}$/J)* mice (stock no. 006148) and *Tg(tet(O)HIST1H2BJ/GFP)47Efu/J*; (stock no. 005104) were purchased from The Jackson Laboratory. *CK5-rtTA* females were crossed to *tet(O)DTA* males to generate a double-transgenic mouse (CK5-DTA) that expresses DTA protein upon doxycycline administration. Aerosolized doxycycline or PBS was administered as described previously[24]. For secretory cell lineage tracing after basal cell ablation, we crossed male *Scgb1a1-creER/Rosa26R-YFP* to CK5-DTA female mice to generate quadruple (SCGB1A1–YFP/CK5-DTA)-transgenic mice. To label secretory cells, we injected tamoxifen intraperitoneally (2 mg per 20 g body weight) for five consecutive days to induce the Cre-mediated excision of a stop codon and subsequent expression of YFP. Both male and female mice were used for experiments. 6–12-week-old mice were used for experiments. Similar aged mice were used for both control and treated animals. We analysed at least three mice per condition in each experiment. The MGH Subcommittee on Research Animal Care approved animal protocols in accordance with NIH guidelines.

SO_2 and influenza infection induced injury. SO_2 injury models have been previously reported[19]. In brief, mice were exposed to 500 p.p.m. of SO_2 for 3 h 40 min. For influenza experiments, influenza A/Puerto Rico/8/34 (PR8) was obtained from Charles River Laboratories International. Mice were anaesthetized and infected with a sublethal dose of influenza by intranasal inhalation as described previously[27]. Mice were killed at day 3 or 14 after infection, and the tracheas were removed and placed in 4% paraformaldehyde (PFA).

Immunofluorescence, microscopy and cell counting. Tracheae were dissected and fixed in 4% PFA for 2 h at 4 °C followed by two washes in PBS, and then embedded in OCT. Cryosections (6 μm) were permeabilized with 0.1% Triton X-100 in PBS, blocked in 1% BSA for 30 min at room temperature (27 °C), incubated with primary antibodies for 1 h at room temperature, washed, incubated with appropriate secondary antibodies diluted in blocking buffer for 1 h at room temperature, washed and counterstained with DAPI. Spheres were fixed with 4% PFA on day 9 after plating and washed with PBS and stained as described above.

The following primary antibodies were used: chicken anti-GFP (1:500; GFP-1020, Aves Labs); rabbit anti-Ki67 (1:200; ab15580, Abcam); rat anti-Ki67 (1:200; 14-5698-82, eBioscience); goat anti-SCGB1A1 (1:500; provided by B. Stripp); mouse anti-p63 (1:100; sc-56188, Santa Cruz); mouse anti-tubulin, acetylated (1:100; T6793, Sigma); mouse anti-FOXJ1 (1:500; 14-9965, eBioscience), rabbit anti-NGFR (1:200; ab8875, Abcam); mouse IgM anti-SSEA-1 (1:100; 14-8813-82, eBioscience); hamster anti-T1α (1:50, DSHB) and rabbit anti-cytokeratin 5 (1:1,000; ab53121, Abcam). All secondary antibodies were Alexa Fluor conjugates (488, 594 and 647) and used at 1:500 dilution (Life Technologies).

Images were obtained using Olympus IX81 Inverted microscope (Olympus). Confocal images were obtained with a Nikon A1 confocal laser-scanning microscope with a 40× or 60× oil objective (Nikon CFI Plan APO VC 40× or 60× Oil). Cells were manually counted based on immunofluorescence staining of markers for each of the respective cell types. Cartilage 1 to 9 was used as reference points in all the tracheal samples to count specific cell types on the basis of immunostaining. Serial sections were stained for the antibodies tested and randomly selected slides were used for cell counting. Percentage of basal cells per sphere was calculated based on CK5 immunostaining. Spheres with less than 2% $CK5^+$ cells were not included in the quantification.

Cell dissociation and sorting. Airway epithelial cells from trachea were dissociated using papain solution. Longitudinal halves of the trachea were cut into five pieces and incubated in papain dissociation solution and incubated at 37 °C for 2 h. After incubation, dissociated tissues were passed through a cell strainer and centrifuged and pelleted at 500*g* for 5 min. Cell pellets were dispersed and incubated with Ovo-mucoid protease inhibitor (Worthington biochemical Corporation, cat. no. LK003182) to inactivate residual papain activity by incubating on a rocker at 4 °C for 20 min. Cells were then pelleted and stained with EPCAM–PECy7 (1:50; 25-5791-80, eBioscience) or EPCAM–APC (1:50; 17-5791, eBioscience), GSIβ4 (*Griffonia Simplicifolia* isolectin beta 4)-Biotin (L2120, Sigma), SSEA-1 eFluor 650NC (1:75, 95-8813-41, eBioscience) and PE anti-mouse CD24 (1:100, 553262, BD Pharmingen) for 30 min in 2.5% FBS in PBS on ice. After washing, cells were sorted on BD FACS Aria (BD Biosciences) using FACS Diva software and analysis was performed using FlowJo (version 10) software.

Sphere-forming assays and transwell cultures. Cells were cultured and expanded in complete SAGM (small airway epithelial cell growth medium; Lonza, CC-3118) containing TGF-β/BMP4/WNT antagonist cocktails and 5 μM Rock inhibitor Y-27632 (Selleckbio, S1049). To initiate air–liquid interface cultures, airway basal stem cells were dissociated and seeded onto transwell membranes. After confluence, media was removed from the upper chamber. Mucocilary differentiation was performed with PneumaCult-ALI Medium (StemCell, 05001). Differentiation of airway basal stem cells on an air–liquid interface was followed by directly visualizing beating cilia in real time after 10–14 days. For clonal culture assays, dedifferentiated basal-like cells ($GSIβ4^+$ YFP^+) were sorted and plated on collagen-coated plates at low cell density to obtain individual colonies. Individual colonies were isolated using microscopic visualization of single colonies followed by trypsin treatment and pipette-assisted aspiration. Individual colony-derived cells were maintained and expanded separately and used for air–liquid interface culture. Sphere culture was performed as described previously[20]. In brief, 50 μl of 1:4 cold Matrigel/MTEC-plus medium was layered on an 8-well chamber slide (Thermo Scientific, cat. no. 177402) and incubated at 37 °C for 10 min to solidify the Matrigel. Sorted cells were mixed in 2% Matrigel in MTEC-plus and plated on pre-coated 8-well chamber slide at a density of 4,000 cells per well. For mixing assays, sorted cells were seeded at a density of 6,000 cells per well. In each experiment, three independent wells were used for each condition tested. Medium was changed every other day for 9 days. For transwells cultures, cells were suspended in MTEC-plus medium and plated on transwell inserts at a cell density of 6,000 cells per well. Medium was changed every day for 7 days. For basal-cell reporter assays, cells were treated with 1 μg ml^{-1} doxycycline either at 24 h after plating or just 24 h before collection. For serial passaging of spheres, medium from culture wells was aspirated, washed with PBS, and then treated with trypsin-EDTA (0.25%) for 2 min. Trypsin was inactivated and dissociated cells were collected and centrifuged at 350*g* for 3 min at 4 °C. Cells were re-seeded at a 1:20 dilution in Matrigel for the next round of sphere culture.

Statistical analysis. The standard error of the mean was calculated from the average of at least three independent tracheal samples unless otherwise mentioned. Data were compared among groups using the Student's *t*-test (unpaired, two-tailed). A *P* value of less than 0.05 was considered significant.

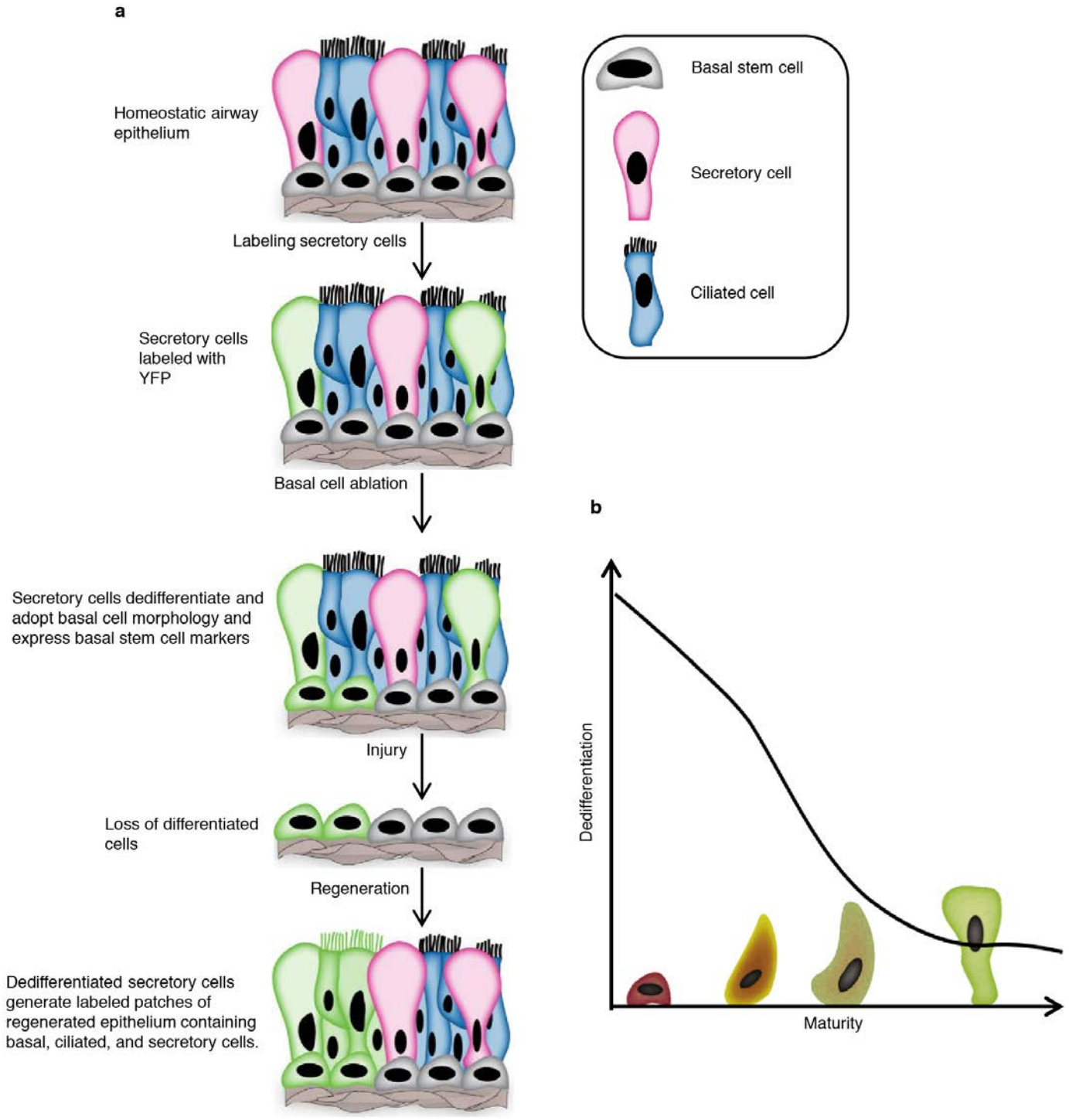

Extended Data Figure 1 | Schematic representation of the dedifferentiation of luminal secretory cells into functional basal stem cells. **a**, Differentiated luminal secretory cells are labelled with a YFP lineage tag in a homeostatic airway epithelium. Basal stem cells are then ablated using diphtheria toxin. In response, lineage-labelled secretory cells dedifferentiate into cells that morphologically resemble basal cells and express basal stem cell markers. These dedifferentiated basal-like cells respond to physiologically relevant toxic and infectious injury and serve as multipotent stem cells during epithelial regeneration. The inset depicts the different cell types of the airway epithelium. **b**, Graphical representation of the dedifferentiation potential of differentiated basal-like cells. *x* axis represents the maturity of a secretory cell; *y* axis represents the propensity for dedifferentiation to a basal-like cell. The propensity to dedifferentiate is inversely correlated to the maturity of the secretory cell.

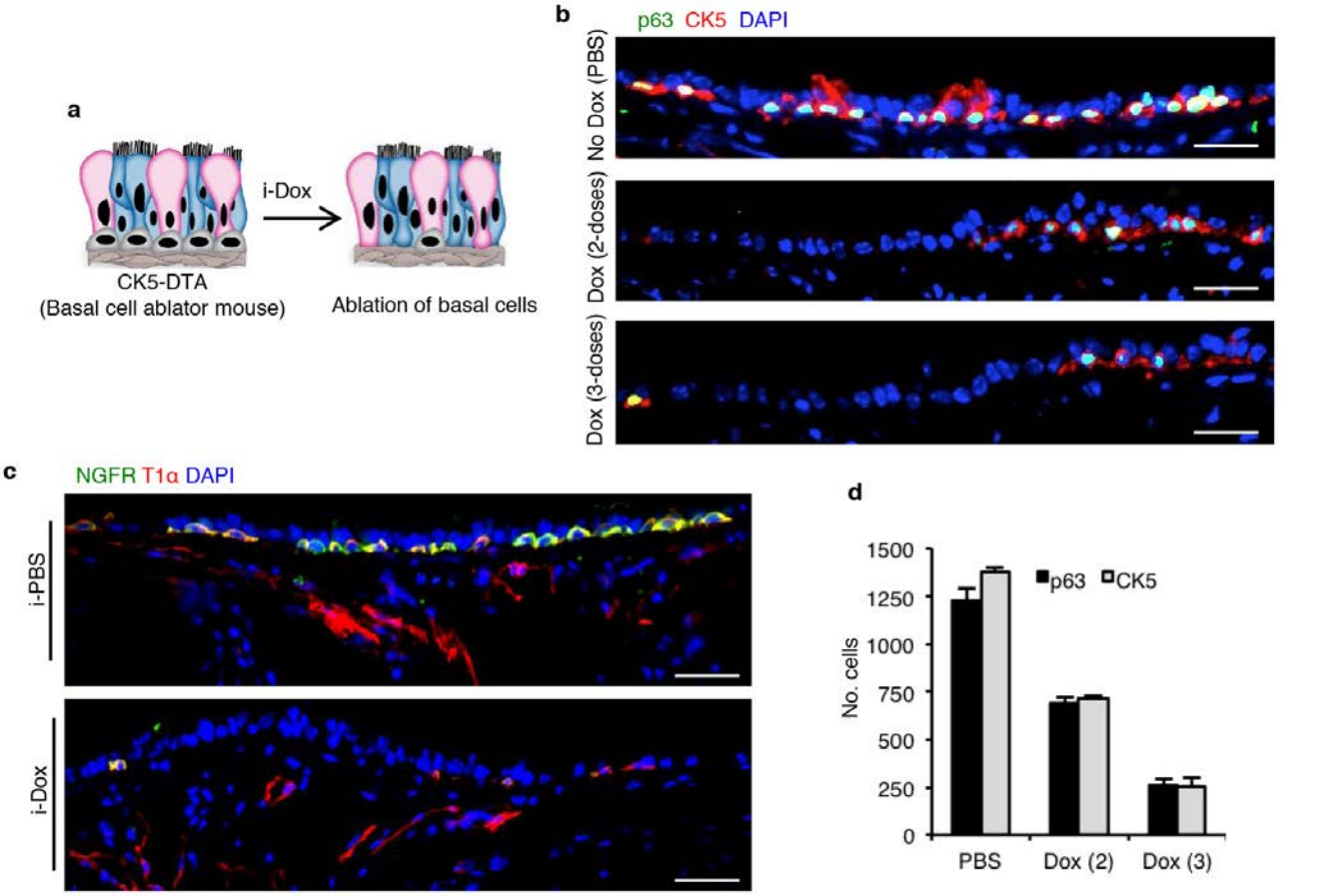

Extended Data Figure 2 | Inhaled doxycycline efficiently ablates basal stem cells of the airway epithelium. **a**, Schematic representation of basal-cell-specific ablation using i-Dox. **b**, Co-labelling of p63 (green) and CK5 (red) on tracheal sections CK5-DTA mice that received either i-PBS (top) or i-Dox (middle and bottom panels show 2 and 3 doses of i-Dox, respectively). **c**, Co-labelling of NGFR (green) and T1α (red) i-PBS- or i-Dox-treated mice. **d**, Quantification of the number of $p63^+$ (black bar) and $CK5^+$ (grey bar) basal cells from CK5-DTA animals treated with PBS (p63, 1,229 ± 65.45; CK5, 1,376 ± 25.23), two doses of i-Dox (p63, 690 ± 35.13; CK5, 716 ± 12.44) or three doses of i-Dox (p63, 262 ± 29.5; CK5, 255 ± 46.82). *y* axis represents the absolute numbers of basal cells (from three independent tracheal sections). Dox(2) and Dox (3) refer to two and three doses of doxycycline inhalation, respectively. $n = 3$ (two mice per condition). Error bars, average ± s.e.m. Scale bars, 20 μm.

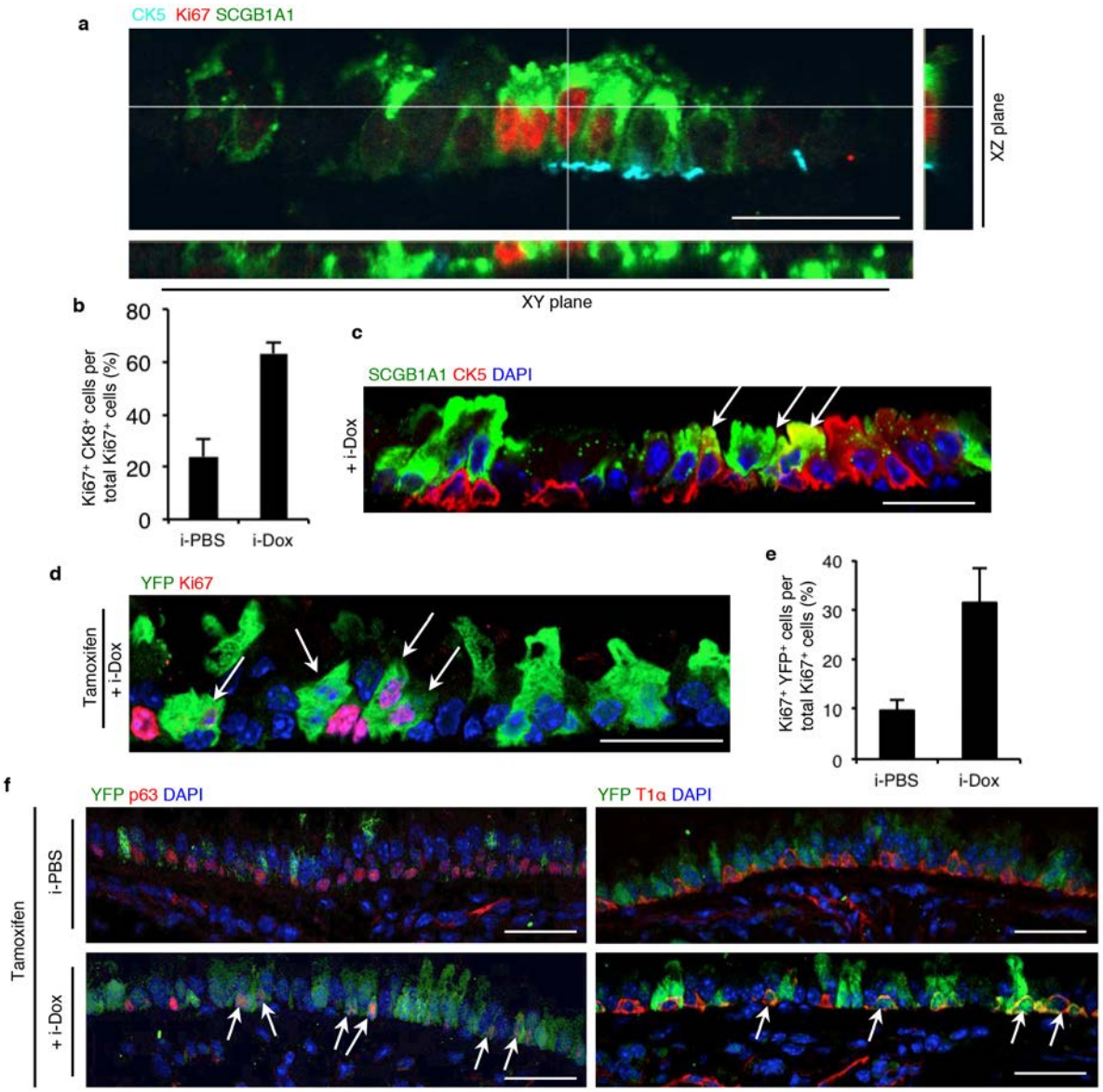

Extended Data Figure 3 | Secretory cells begin to express proliferation and stem cell markers and undergo dedifferentiation following basal cell ablation. **a**, Orthogonal confocal optical sections of SCGB1A1 (green), CK5 (cyan) and Ki67 (red) XY and XZ planes are shown to demonstrate the colocalization of Ki67 and SCGB1A1. **b**, Quantification of the percentage of $Ki67^+$ $CK8^+$ double-positive cells per total $Ki67^+$ cells from i-PBS (23.74% ± 6.76)- and i-Dox (63.22% ± 4.14)-treated CK5-DTA mice. **c**, Co-labelling of CK5 and SCGB1A1 in i-Dox-treated CK5-DTA mice. White arrows, double-positive cells. **d**, Immunostaining for YFP (green) and Ki67 (red) on sections from SCGB1A1–YFP/CK5-DTA mice. White arrows indicate YFP^+ $Ki67^+$ cells. **e**, Quantification of the percentage of YFP^+ $Ki67^+$ cells per total $Ki67^+$ cells in SCGB1A1–YFP/CK5-DTA mice that were treated with either i-Dox (31.74% ± 7.15) or i-PBS (9.65% ± 2.12). **f**, Co-labelling of YFP (green) with p63 or T1α (red) on tracheal sections of SCGB1A1–YFP/CK5-DTA mice that were either treated with i-PBS (top) or i-Dox (bottom). White arrows, double-positive cells. $n = 3$ (three mice per condition). Error bars, average ± s.e.m. Scale bars, 20 μm.

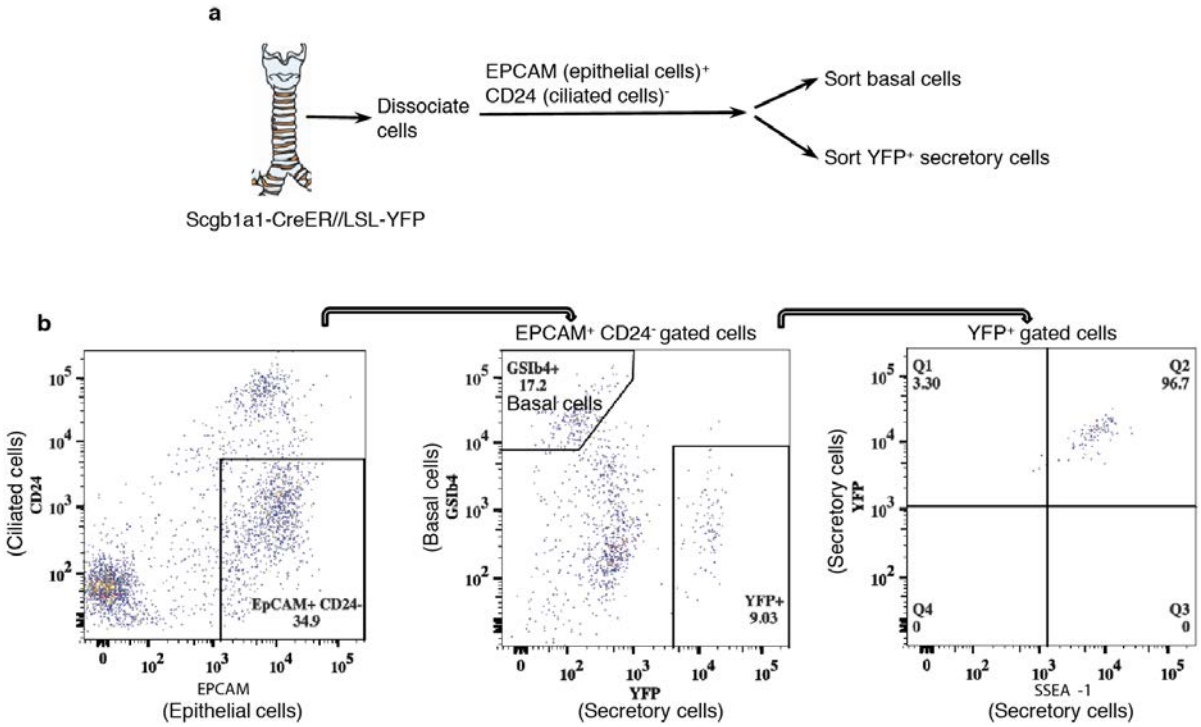

Extended Data Figure 4 | Dissociation and fluorescence activated cell sorting of airway epithelial cells. **a**, Schematic representation of tracheal epithelial cell dissociation from secretory cell lineage-labelled mice (SCGB1A1-CreER/LSL-YFP) after five doses of tamoxifen. Of the total epithelial cells, $EPCAM^+$ $CD24^-$ cells were gated to remove ciliated cells. Then YFP^+ secretory cells and $GSI\beta4^+$ basal cells were sorted. **b**, Of the total epithelial cells, $EPCAM^+$ $CD24^-$ cells were gated to remove ciliated cells (left). Then, YFP^+ secretory cells were separated from $GSI\beta4^+$ basal cells (middle). Sorted YFP^+ cells were also marked by the secretory cell marker SSEA-1 as expected for a pure population of $SCG1A1^+$ cells (right).

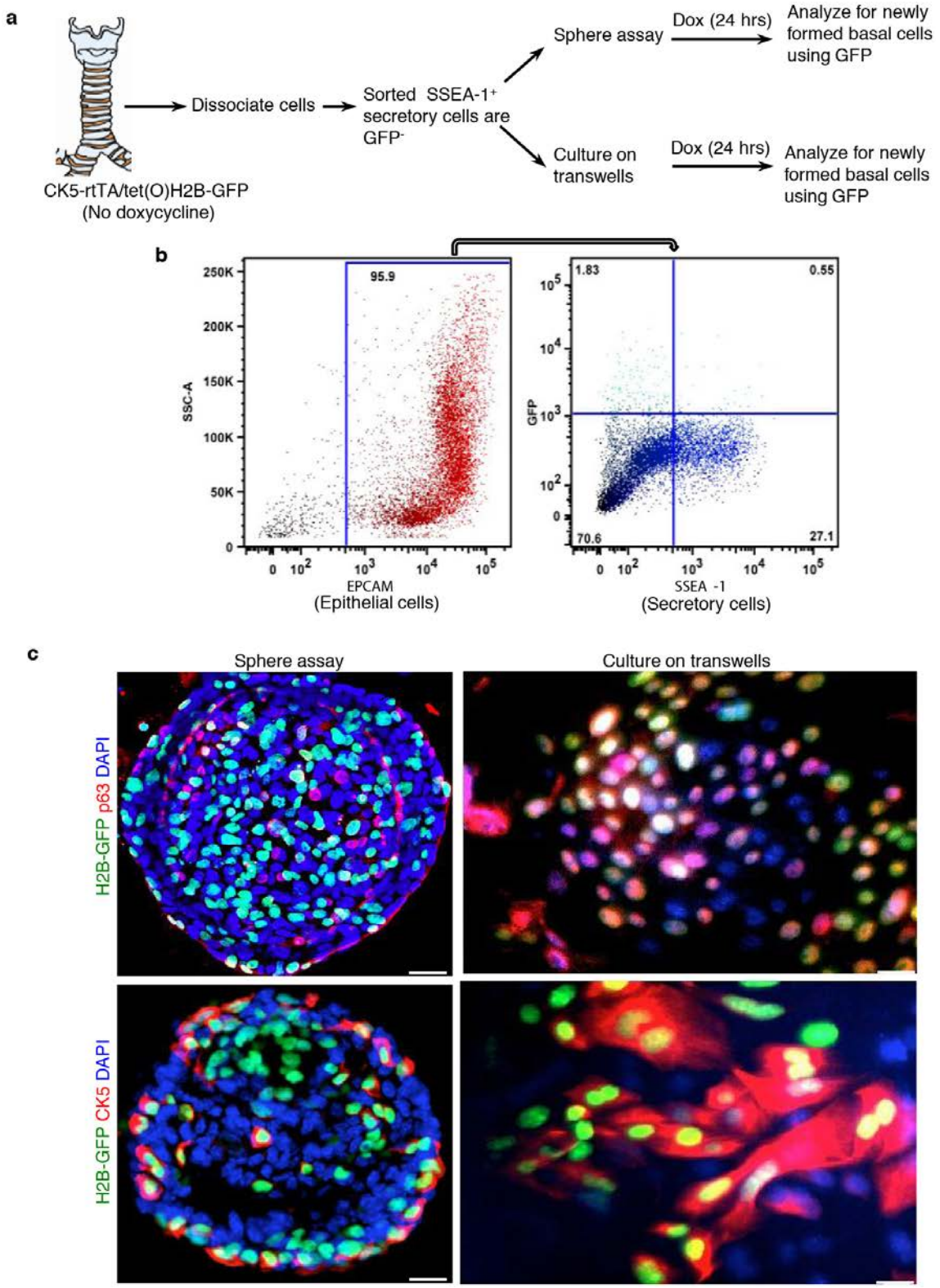

Extended Data Figure 5 | Sorted secretory cells dedifferentiate into basal-like self-renewing stem cells upon *ex vivo* culture. **a**, Schematic representation of tracheal epithelial cell dissociation from basal cell reporter mice (*CK5-rtTA/tet(O)H2BGFP*) followed by sorting of GFP–SSEA-1$^+$ secretory cells. Sorted SSEA-1$^+$ cells were grown as spheres in Matrigel or plated on transwell membranes. Doxycycline was administered and cells were monitored for the initiation of GFP expression. **b**, Fluorescence-activated cell sorting of SSEA-1$^+$ cells from basal cell reporter mice (*CK5-rtTA/tet(O)H2BGFP*). Arrows indicate gating windows. EPCAM is a pan-epithelial marker used to exclude non-epithelial lineages. Sorted SSEA-1$^+$ secretory cells did not express GFP. **c**, Immunofluorescence staining for p63 (red; top) or CK5 (red; bottom) in combination with H2B–GFP (green; all panels) on sorted secretory cells that were either cultured as Matrigel spheres (left) or on transwells (right). Immunofluorescence analysis confirmed that H2B–GFP$^+$ cells expressed p63 and CK5, again confirming that secretory cells dedifferentiate in culture. $n = 3$ (two replicates per condition). Scale bars, 20 μm.

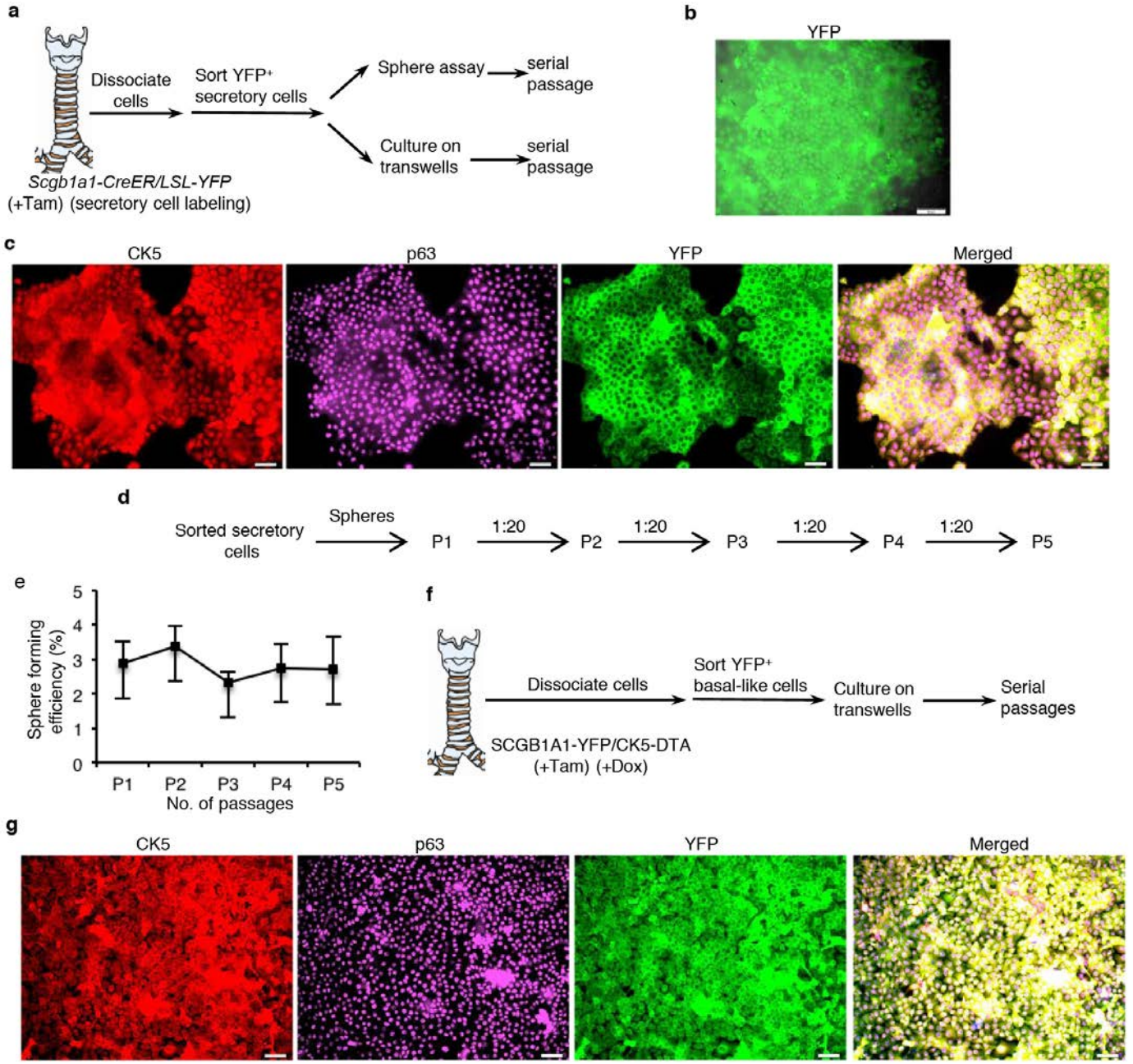

Extended Data Figure 6 | Sorted lineage-labelled secretory cells undergo dedifferentiation *ex vivo*, express basal stem cell markers, and can be serially passaged, as can secretory cells that underwent dedifferentiation *in vivo*. **a**, Schematic representation of secretory cell labelling, sorting and subsequent culturing in Matrigel or on transwell membranes. **b**, Cell colonies obtained from early passage cultures of YFP^+ secretory-cell-derived cells on transwell membranes. **c**, Immunostaining for CK5 (red), p63 (magenta) and YFP (green) on passage-five basal cell colonies from *ex vivo*-dedifferentiated cells. **d**, Schematic showing that YFP^+ secretory-cell-derived spheres from SCGB1A1-CreER/LSL-YFP mice were serially passaged for five generations. **e**, Quantification of the sphere-forming efficiency: P1 (2.86% ± 0.65), P2 (3.36% ± 0.6), P3 (2.31% ± 0.32), P4 (2.75% ± 0.69) and P5 (2.7% ± 0.94). *x* axis, number of passages. *y* axis, percentage of spheres formed. **f**, Schematic representation of *in vivo* dedifferentiation followed by the sorting and culturing of YFP^+ basal-like cells. **g**, Immunostaining for CK5 (red), p63 (magenta) and YFP (green) on passage-five cell colonies from *in vivo*-dedifferentiated cells. $n = 3$ (two replicates per condition). Error bars, average ± s.e.m. Scale bars, 20 μm.

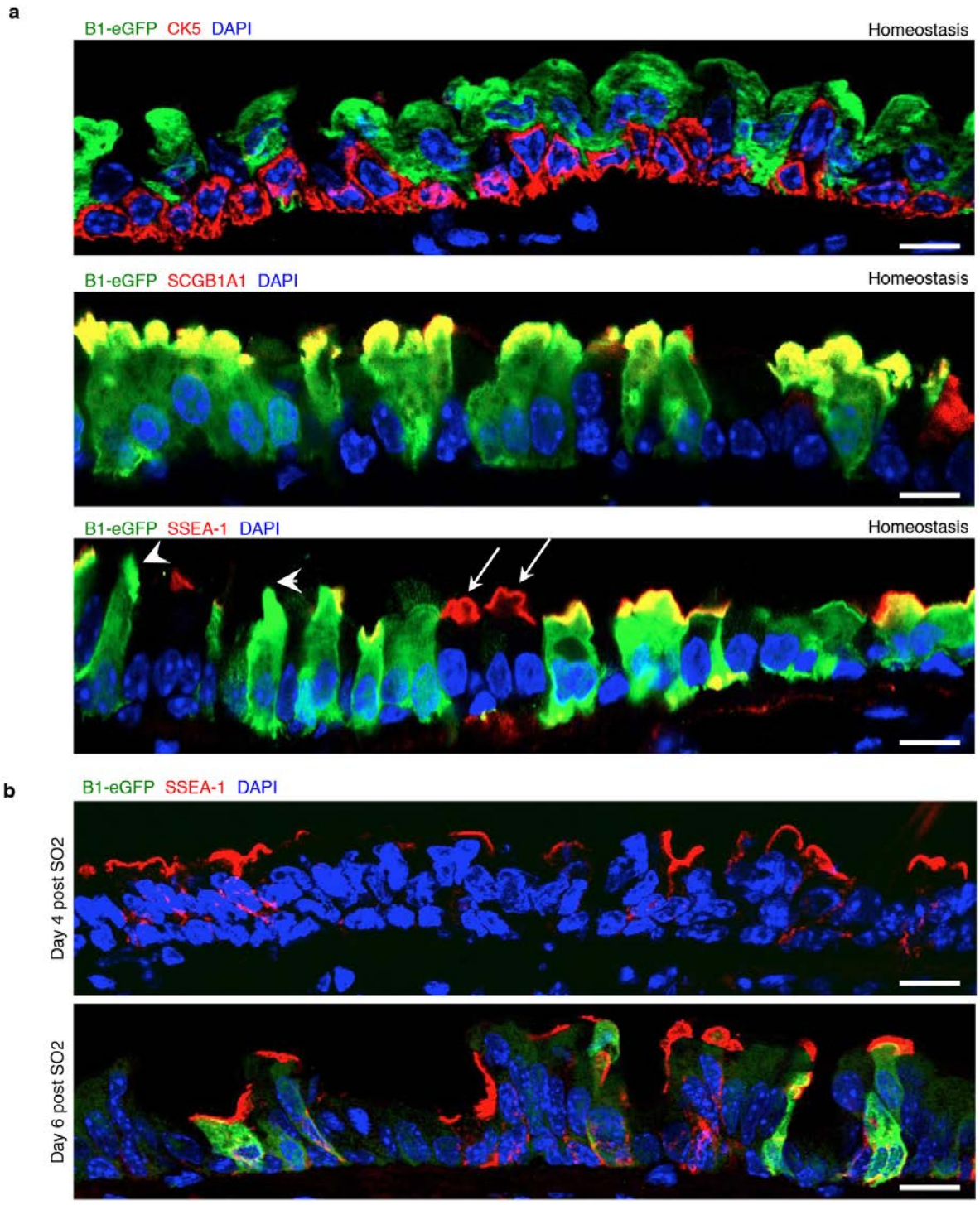

Extended Data Figure 7 | B1–eGFP transgenic mice express GFP in mature subsets of secretory cells. **a**, Co-labelling of GFP (green) with CK5 or SCGB1A1 or SSEA-1 (all in red) on large airways sections derived from adult B1–eGFP transgenic mice at homeostasis. White arrows indicate SSEA-1^{+} B1–eGFP^{-}, whereas white arrowheads point to cells that are B1–eGFP^{+} SSEA-1^{-} (bottom). **b**, B1–eGFP trachea were stained for GFP (green) and SSEA-1 (red) on day 4 and day 6 after SO_2-induced injury. $n = 3$ (two mice per condition per time point). Scale bars, 20 μm.

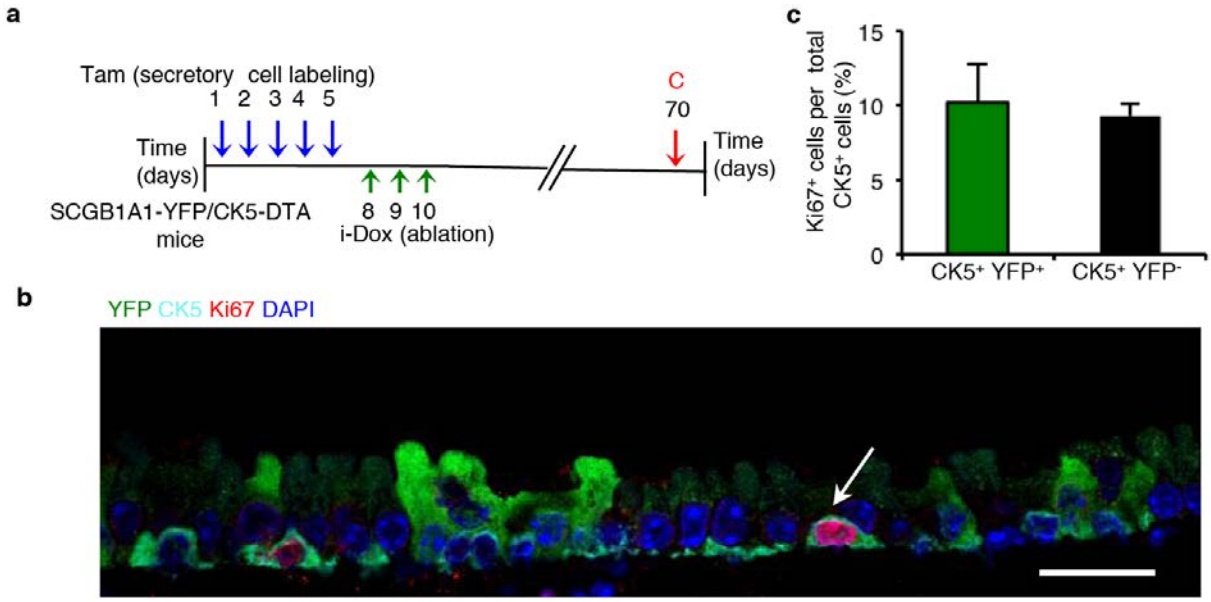

Extended Data Figure 8 | Dedifferentiated basal-like stem cells are stable and self-renew to the same degree as endogenous basal stem cells. **a**, Schematic representation of the dedifferentiation protocol to assess the ability of basal-like stem cells to persist and self-renew for 2 months. **b**, Immunofluorescence staining for YFP (green) in combination with CK5 (cyan) or Ki67 (red) on sections from SCGB1A1–YFP/CK5-DTA mice 2 months after basal cell ablation. **c**, Quantification of the percentage of proliferating dedifferentiated $CK5^+$ YFP^+ (10.16% ± 2.57) (green bar) and wild-type $CK5^+$ YFP^- (9.25% ± 0.79) (black bar) stem cells out of the total $CK5^+$ stem cell population in the large airways of SCGB1A1–YFP/CK5-DTA mice 2 months after basal cell ablation. The white arrow points to a proliferating dedifferentiated basal-like stem cell. $n = 3$ (two mice per condition). Error bars, average ± s.e.m. Scale bar, 20 μm.

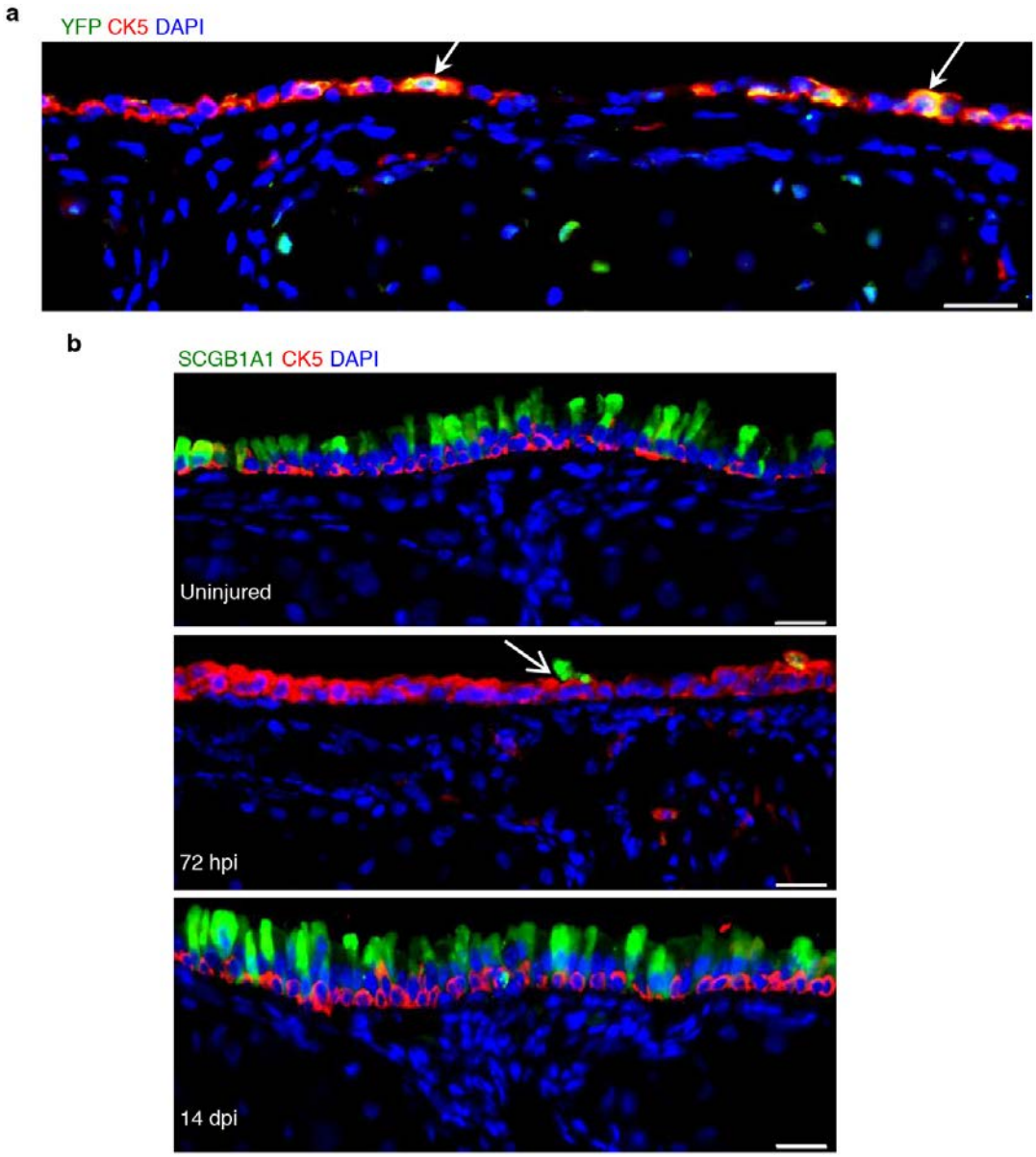

Extended Data Figure 9 | SO_2-and influenza-induced injury efficiently removes the suprabasal cells of the airway epithelium.
a, Immunofluorescence staining for CK5 (red) and YFP (green) in SCGB1A1–YFP/CK5-DTA airway epithelium 24 h after SO_2 inhalation. Only a single layer of basal cells persists after injury. White arrows, $CK5^+$ YFP^+ double-positive cells (yellow). **b**, Immunofluorescence analysis of basal cells (CK5, red) and secretory cells (SCGB1A1, green) from uninjured (top), 72 hours post-infection (h.p.i.; middle) and 14 days post-infection (d.p.i.; bottom). White arrow, secretory cell debris (in green). $n = 3$ (two replicates per condition). Scale bars, 20 μm.

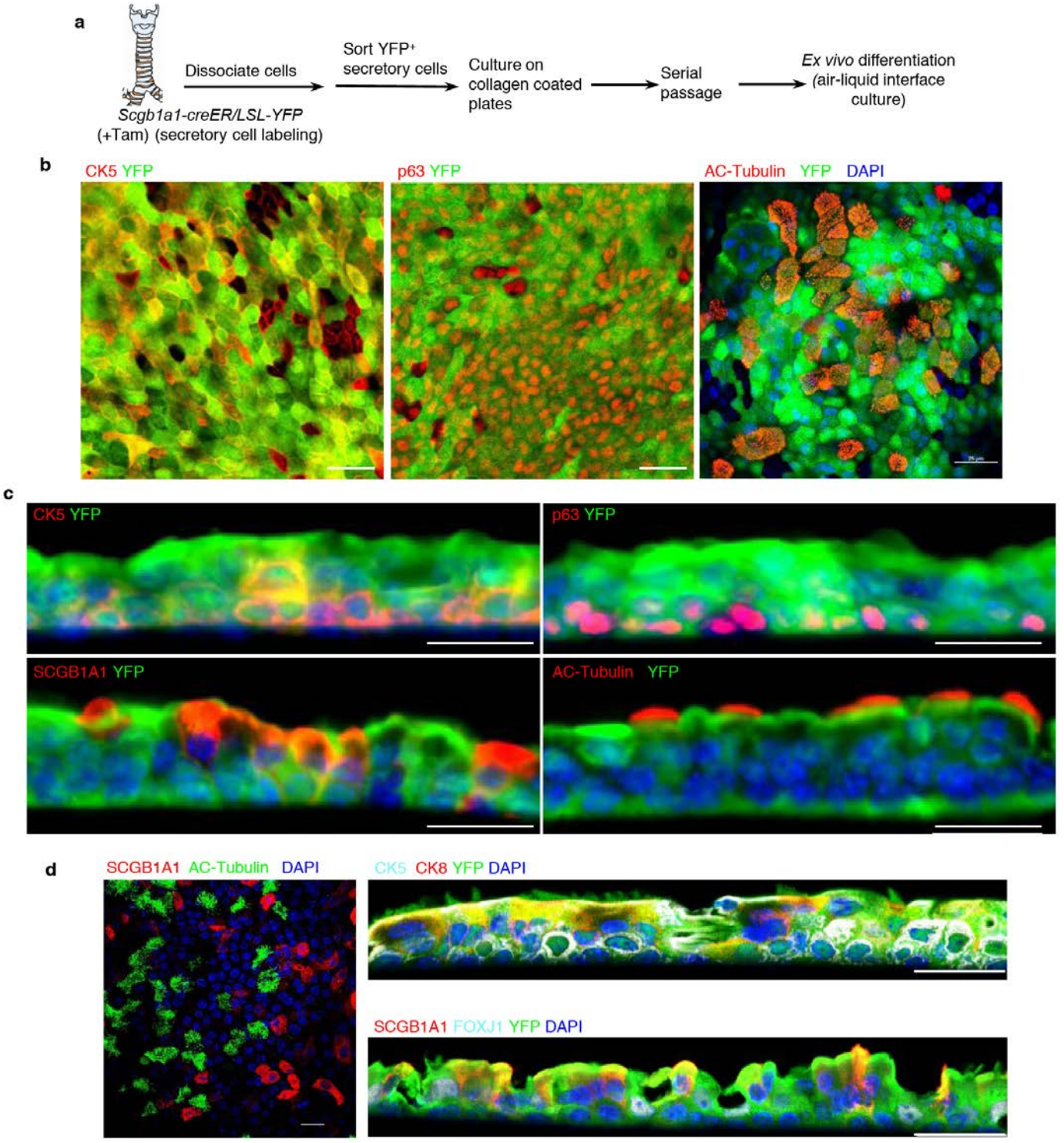

Extended Data Figure 10 | *Ex vivo*-dedifferentiated cells can be clonally expanded and give rise to a complete airway epithelium in air–liquid interface cultures. **a**, Schematic representation of the *ex vivo* dedifferentiation of secretory cells, serial passage and differentiation. **b**, Whole-mount immunostaining for YFP (green) in combination with CK5 or p63 or acetylated (AC)-tubulin (red). **c**, Co-labelling of YFP (green) with CK5 or p63 or SCGB1A1 or acetylated-tubulin (red) on differentiated epithelium derived from serially passaged dedifferentiated basal-like cells. **d**, Whole-mount immunofluorescence staining for SCGB1A1 (red) and acetylated-tubulin (green) on clonally derived epithelium (left). Co-labelling of YFP (green) with CK5 (white) and CK8 (red; top) or SCGB1A1 and FOXJ1 (bottom) on cross sections of clonally derived epithelium. Scale bars, 20 μm.